AGU ADVANCING EARTH AND SPACE SCIENCE

Geophysical Research Letters®

Key Points:

- Around the minimum storm-time SYM-H, Magnetospheric Multi-Scale encountered different magnetopause boundary layers (BLs) with multiple entries into the magnetosphere
- Bz remains negative during one magnetopause crossing, indicating an encounter with the magnetosphere in the vicinity of the southern cusp
- Observations and global simulations support that secondary reconnection near the southern cusp produces closed BL magnetic flux

Correspondence to:

B. L. Burkholder,
burkbran@umbc.edu

Author Contributions:

Conceptualization: Brandon L. Burkholder
Data curation: Brandon L. Burkholder
Formal analysis: Brandon L. Burkholder
Funding acquisition: Brandon L. Burkholder
Investigation: Brandon L. Burkholder
Methodology: Brandon L. Burkholder
Project Administration: Li-Jen Chen
Resources: Brandon L. Burkholder
Software: Brandon L. Burkholder, Jason Shuster
Supervision: Li-Jen Chen

MMS Observations of Storm-Time Magnetopause Boundary Layers in the Vicinity of the Southern Cusp

Brandon L. Burkholder[1,2] , Li-Jen Chen[2] , Stephen Fuselier[3,4] , Daniel Gershman[2] , Conrad Schiff[2], Jason Shuster[2,5] , Ying Zou[6], Brian M. Walsh[7] , Patricia Reiff[8] , Steve Petrinec[9] , and Anthony Sciola[10]

[1]Goddard Planetary Heliophysics Insitute, University of Maryland Baltimore County, Baltimore, MD, USA, [2]NASA Goddard Space Flight Center, Greenbelt, MD, USA, [3]Space Science and Engineering Department, Southwest Research Institute, San Antonio, TX, USA, [4]University of Texas at San Antonio, San Antonio, TX, USA, [5]Department of Astronomy, University of Maryland, College Park, Baltimore, MD, USA, [6]Department of Space Science, University of Alabama in Huntsville, Huntsville, AL, USA, [7]Center for Space Physics, College of Engineering, Boston University, Boston, MA, USA, [8]Physics and Astronomy Deptartment, Rice University, Houston, TX, USA, [9]Advanced Technology Center, Lockheed Martin, Palo Alto, CA, USA, [10]Johns Hopkins University Applied Physics Laboratory, Laurel, MD, USA

Abstract During a storm-time interval around winter solstice, observations by the Magnetospheric Multi-Scale (MMS) Mission show multiple distinct magnetopause boundary layers (BLs) in the vicinity of the southern cusp. The microphysics of the solar wind-magnetosphere interaction during storm times are not well understood, because the observations are relatively lacking. This event enables the opportunity to probe the storm-time magnetopause, and observations support that MMS was near a reconnection site equatorward of the southern cusp, suggesting active reconnection in close proximity to closed magnetic flux regions in the BL. The Grid Agnostic magnetohydrodynamics (MHD) for Extended Research Applications global MHD simulation shows evidence for transient secondary reconnection sites near the southern cusp, demonstrating mechanisms to form closed field line regions of the BL.

Plain Language Summary The physical processes by which the solar wind plasma penetrates Earth's magnetic shield are hotly debated. Furthermore, it is even less understood how the solar wind-magnetosphere interaction plays out during geomagnetic storms, since observations are harder to obtain. Large geomagnetic storms sparked by strong solar activity occur only a few times yearly, and planning spacecraft observations during these times is extremely difficult. Fortunately, the Magnetospheric Multi-Scale spacecraft constellation obtained storm-time observations which provide the opportunity to reveal properties of the disturbed outer magnetosphere, in particular, at the interface of solar wind and geomagnetic fields. The event in this study shows magnetic reconnection occurring in an unusual location, which helps to understand the possible origin of the different observed boundary layers and how plasma is transported across them.

1. Introduction

For southward interplanetary magnetic field (IMF), day-side reconnection produces a low-latitude magnetopause BL composed of newly reconnected magnetic flux. On the magnetosheath side, the magnetosheath boundary layer (MSBL) contains both magnetosphere and magnetosheath plasma (Cowley, 1982; Eastman & Hones, 1979; Mitchell et al., 1987). At the low-shear magnetopause, electrons above 50 eV can be used as an indicator of the transition from magnetosheath to MSBL, due to the changing topological connection (Fuselier et al., 1997). The low-latitude boundary layer (LLBL; Nakamura, 2021), composed of magnetospheric reconnected field lines, is where the solar wind plasma penetrates Earth's magnetosphere. The purpose of this study is to illuminate the physics of these boundaries layers during geomagnetic storms.

Typically, geomagnetically disturbed periods are characterized by enhanced entry of plasma, stronger convection, and more magnetospheric transport. Although, less is known about the magnetopause BLs during strong disturbances, since the number of useful observations is limited by the frequency of storms, occurring at about 20/year (Reyes et al., 2021). For a moderate storm, Sonnerup (1971) reported an Explorer-12 crossing of both the MSBL and LLBL, providing early evidence for the open magnetosphere model. Maynard et al. (1991) studied BL dynamics during a storm based on multi-spacecraft observations and concluded that the x-line extended over a significant range of local time, allowing the magnetosheath plasma access into the magnetosphere over this range.

Validation: Brandon L. Burkholder
Visualization: Brandon L. Burkholder, Jason Shuster
Writing – original draft: Brandon L. Burkholder
Writing – review & editing: Brandon L. Burkholder, Li-Jen Chen, Stephen Fuselier, Conrad Schiff, Jason Shuster, Ying Zou, Brian M. Walsh, Patricia Reiff, Steve Petrinec, Anthony Sciola

Farrugia et al. (2017) and Paschmann et al. (2021) examined low Mach number magnetopause BL traversals associated with storm-time. The event discussed in Section 3 examines the transition from storm-time BL into the exterior cusp magnetosphere for the first time.

Global simulation studies are a vital tool for understanding storm-time BLs because of the dynamics of the system (i.e., expanding/contracting magnetosphere C. Wang et al. (2005) and Li et al. (2011)) and the inclusion of global effects (i.e., reconnection and Kelvin-Helmholtz instability). For instance, Brenner et al. (2021) quantified energy transport across the entire magnetopause during a large geomagnetic storm and also reproduced the boundary motions observed by multiple spacecraft. But the available resolution for global simulations is low compared to scales that modern observational platforms have access to, and local simulations cannot reproduce BL behavior unless they include either a detailed or a phenomenological model. At high-latitude in particular, the BL is not well resolved in global simulations (Michael et al., 2021).

Fortunately, near the minimum SYM-H of the 2015 winter solstice storm, the Magnetospheric Multiscale (MMS) spacecraft gathered measurements of BLs near the southern cusp. This storm, which was associated with an interplanetary coronal mass ejection, reached a maximum storm-time planetary Kp index of 7 and was classified as G2 on the NOAA scale. Notably, Fuselier et al. (2019) used this event in a statistical study of the warm plasma cloak. Here, we report MMS storm-time BL observations during low Mach number solar wind conditions and large dipole tilt, showing also nearby reconnection in the vicinity of the southern cusp that has been previously postulated as a source of closed BL flux during similar magnetospheric conditions. A description of the observational data sets used is given in Supporting Information S1. We also employ a three-dimensional global magnetosphere simulation to help understand the origin and magnetic connection of storm-time BLs observed by MMS.

2. Boundary Layer Observations Near the Southern Cusp

Figure 1 (bottom) shows in the geocentric solar magnetospheric (GSM) coordinate system, the z position of MMS was $-1.7 R_E$, but these observations are near winter solstice with dipole tilt $-24.2°$ (Nowada et al., 2009). Thus, although MMS was just southward of the GSM equatorial plane, the spacecraft was able to encounter the low-latitude edge of the southern exterior cusp region. OMNI data indicated strongly southward IMF $B_z \sim -15$ nT lasting from 15:00 UT 12/20 to 4:00 UT 12/21, with B_x mostly at -5 nT. During the time of interest, 22:10–23:59 UT 12/20, the IMF B_y (Figure 1a) was first slightly positive (2–3 nT) as MMS crossed from the region labeled sheath to BL1 (BL 1: preferred nomenclature is BL rather than MSBL or LLBL because these are storm-time BLs not sharing all the characteristics of known BLs). After 23:00 UT, when MMS encountered the magnetosphere a few times, the IMF B_y component was slightly negative. Around 22:50 UT the SYM-H index (Figure 1b, red trace left axis) reached storm-time low at ~ -170 nT, indicating the end of the storm main phase, just a few minutes after MMS first crossed from magnetosheath into BL1. The solar wind Alfvén Mach number (Figure 1b, black trace right axis) is ≤ 2 when MMS is in the BL and magnetosphere and approaches 1 at 23:30 UT, indicating a nearly sub-Alfvénic solar wind.

Colored highlighting from Figure 1 represents the distinct regions encountered by MMS during its outbound orbit, as boundary motions moved it from the magnetosheath (yellow), through BL1 (red), and into a magnetosphere region (no highlight) with $B_z < 0$. The BL regions are formed by primary reconnection north of the spacecraft. The basis of this interpretation is as follows. The ion energy spectrogram (Figure 1c) shows in the first magnetosheath region a population having peak energy at 200–300 eV which abruptly increases to ~ 1 keV, then decreases back to 300–400 eV in BL1. Magnetosheath ions below 50 eV are energized in BL1. Electrons (Figure 1d) in the magnetosheath have 100 eV peak energy, while in BL1 some intervals show higher-than-sheath energy electrons. Furthermore, both the plasma characteristics and magnetic field strength in BL1 (approximately half the magnetosheath value) are consistent with those in the BL produced by reconnection exhausts reported in Paschmann et al. (2021).

The crossing from BL1 to the magnetosphere is characterized by (a) increase of peak ion energy to ≥ 10 keV, (b) increase of the peak electron energy up to 1 keV, and (c) energetic (70–1,000 keV) electron flux at pitch angles with enhancements at $50°–130°$ (Figure 1e). The thermal plasma energy change is 2(1) orders of magnitude increase from BL1 to magnetosphere for the ions(electrons). Note all three magnetic field components exhibit a sharp transition as MMS enters the magnetosphere, even though $B_z < 0$ (Figure 1f).
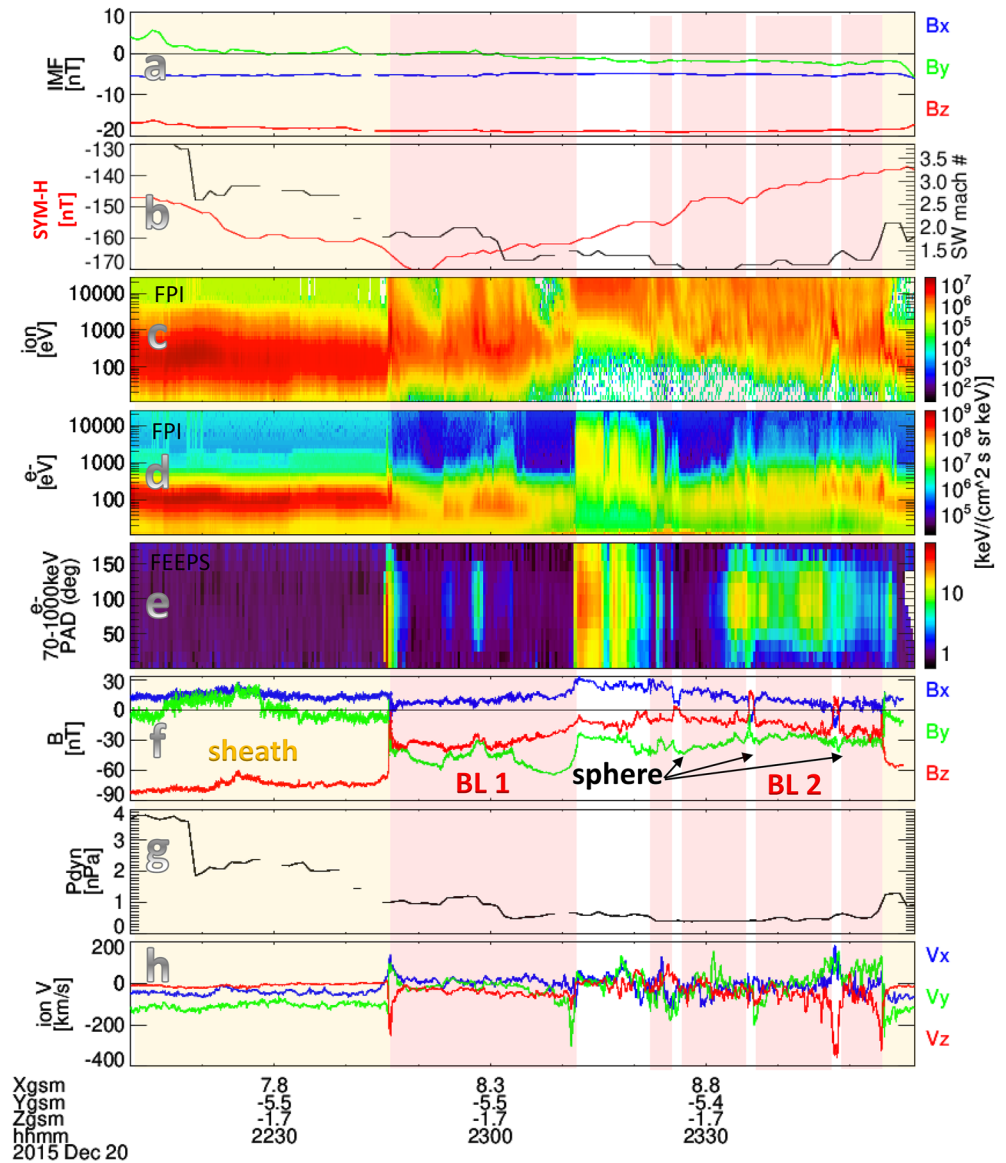
Figure 1. Overview of MMS1 storm-time boundary layer (BL) observations. Panels show OMNI interplanetary magnetic field (a), SYM-H index (left axis, red trace, panel (b)) and OMNI solar wind Alfvén Mach number (right axis, black trace, panel (b)), Fast Plasma Investigation (FPI) omni-directional ion (c) and electron (d) spectrograms, Fly's Eye Energetic Particle Spectrometer electron pitch angle distribution (e), Fluxgate Magnetometer magnetic field vector (f), OMNI dynamic pressure (g), FPI ion velocity vector (h). Highlighting shows magnetosheath (yellow), BL (red), and magnetosphere (none). Vector quantities are in geocentric solar magnetospheric coordinates.

Eventually, MMS passed back through the BL (BL2 in Figure 1), encountering more magnetosheath at the end of the interval, with a few short excursions into the positive B_z magnetosphere. The initially outward boundary motion corresponds to decreasing dynamic pressure (Figure 1g) in OMNI data starting at ~22:20 UT. The dynamic pressure enhancement at the end of the interval also corresponds with the inward boundary motion required to bring MMS back to magnetosheath around 23:55 UT.

When MMS left the magnetosphere around 23:23 UT, it encountered the region labeled BL2. An even larger portion of both magnetosheath ions and electrons, compared to BL1, are energized in BL2. Shortly after crossing from magnetosphere to BL2, B_z reverses at 23:26 UT, and later has two strong reversals about 1 min long, correlated with features in the Fast Plasma Investigation (FPI) ion and electron spectrograms as well as strong plasma flows (Figure 1h). These are short crossings into the magnetosphere side of the magnetopause. At around

23:55 UT MMS moves back into the magnetosheath. Figure 1e shows a 0°–120° burst of energetic electrons as MMS passes from magnetosheath to BL1, but electrons are otherwise absent at these energies in the magnetosheath. In BL1 and BL2, where Fly's Eye Energetic Particle Spectrometer (FEEPS) fluxes are enhanced the pitch angles are peaked at 90°, with more intense fluxes in BL2. These magnetospheric electron signatures in the BL indicate regions of closed magnetic field topology (Paschmann et al., 2021). During the first magnetosphere encounter (under negative B_z), the distribution has higher fluxes at 0° and 180° pitch angles, compared to most of BL1 and BL2, also consistent with closed field lines in the magnetosphere. The signatures of these wide magnetopause BLs are not typical of a crossing from magnetosheath to magnetosphere, and have been observed during storm-time with similar low Mach number (1–2) solar wind and also during large dipole tilt (Paschmann et al., 2021).

One key new feature in the storm-time BL observations presented in Figure 1 and not in the report by Paschmann et al. (2021) is the entry into the magnetosphere with $B_z < 0$. Two possible scenarios may be admitted to account for the unusual magnetosphere entry: (1) from BL1 through the magnetopause equatorward of the southern cusp; (2) from BL1 into the magnetosphere tailward of the southern cusp. Scenarios 1 and 2 are illustrated in Figure 4a as the black and orange trajectories (dashed lines) crossing the green (BL) into the blue and magenta (closed magnetosphere) field lines, respectively.

Figure 2 further characterizes the storm-time BLs from 22:40 to 23:59 UT. The vertical dashed green lines in Figures 2a–2c illustrate each magnetosheath-to-BL crossing. The FPI omni-directional ion spectrogram (Figure 2a) shows both regions aligned with positive B_z (Figure 2b) contain a less dilute mixture of the magnetospheric and magnetosheath plasma. Figure 2c showing Hot Plasma Composition Analyzer O+ density, leads to the conclusion that everywhere between the green lines is magnetically connected to at least one hemisphere.

Figures 2d–2i present zoomed-in views of two intervals where MMS observes unequal fluxes of parallel and anti-parallel electrons. The electron velocity distribution Figure 2d is sliced in a magnetic field parallel-perpendicular (⊥1 defined by $\mathbf{E} \times \mathbf{B}$, see Shuster et al. (2019)) plane and taken from the time marked by the vertical line in Figure 2e, just before the boundary crossing from BL1 to the magnetosphere. The parallel and anti-parallel energy spectrograms in Figures 2e and 2f show enhanced fluxes at energies >1 keV in the parallel direction but not anti-parallel, at 23:11–23:12 UT. Given that $B_z < 0$, $B_y(<0)$ is dominant (Figure 1d), and $V_{iy} \sim -300$ km/s, we interpret the uni-directional parallel electrons above 1 keV as coming from a reconnection site duskward and earthward of MMS under scenario 1 (black x in Figure 4b), and duskward and northward (equatorward) of MMS under scenario 2 (orange x in Figure 4a).

The BL2-to-magnetosphere crossing occurred under a positive B_z, and hence this magnetosphere must be equatorward of the cusp. The parallel and anti-parallel energy spectrograms in Figures 2g and 2h are observed in burst mode and they show >1 keV field-aligned uni-directional electrons at 23:35:50–23:35:55 UT, with other patchy intervals prior to that. We interpret these electrons as coming from a reconnection site duskward and earthward of MMS, as B_y is dominant and $B_z < 0$ (Figure 1f). The burst distribution (Figure 2i) taken from the time marked by the vertical dashed line in Figures 2g and 2h shows that the low- and mid-energy electrons are actually more anti-field-aligned where the heated electrons are field-aligned. Furthermore, the distribution exhibits perpendicular heating, consistent with the reconnection exhaust not too far from the x-line (Lavraud et al., 2016; Shuster et al., 2014). Figure 3 further explores this possibility. Local reconnection signatures would suggest the regions of positive B_z embedded in BL2 would not be closed magnetospheric flux. However, note that FEEPS electrons (Figure 1) show enhanced fluxes at 0° and 180° during these B_z reversals, similar to the magnetosphere observed under negative B_z, therefore we label these regions magnetosphere.

During the strong positive B_z excursion embedded in BL2 around 22:36 UT, MMS observed features suggesting close proximity to a reconnection site near the southern cusp. Figure 3 shows burst mode observations from 23:35:45 to 23:36:15 UT. Figure 3a shows B_x and B_z reverse around 23:36:00 UT, also associated with reversals of the ion velocity components V_x and V_z (Figure 3b). Where B_x and B_z approach zero there is a −10 nT B_y. Figure 3c shows a local density minimum occurs simultaneously with the start of (a) B_y decrease, (b) enhancements of 1–10 keV ion flux (Figures 3d) and 0.1–1 keV electron flux (Figure 3e), (c) stronger parallel >1 keV electron flux around 23:35:54 (Figure 3f, black box) and stronger anti-parallel >1 keV electron flux around 23:26:08 (Figure 3g, black box), which are electrons accelerated near the reconnection site streaming along magnetic field lines near the separatrix, (d) enhanced electric field fluctuations (Figure 3h), and (e) unmagnetized ions along
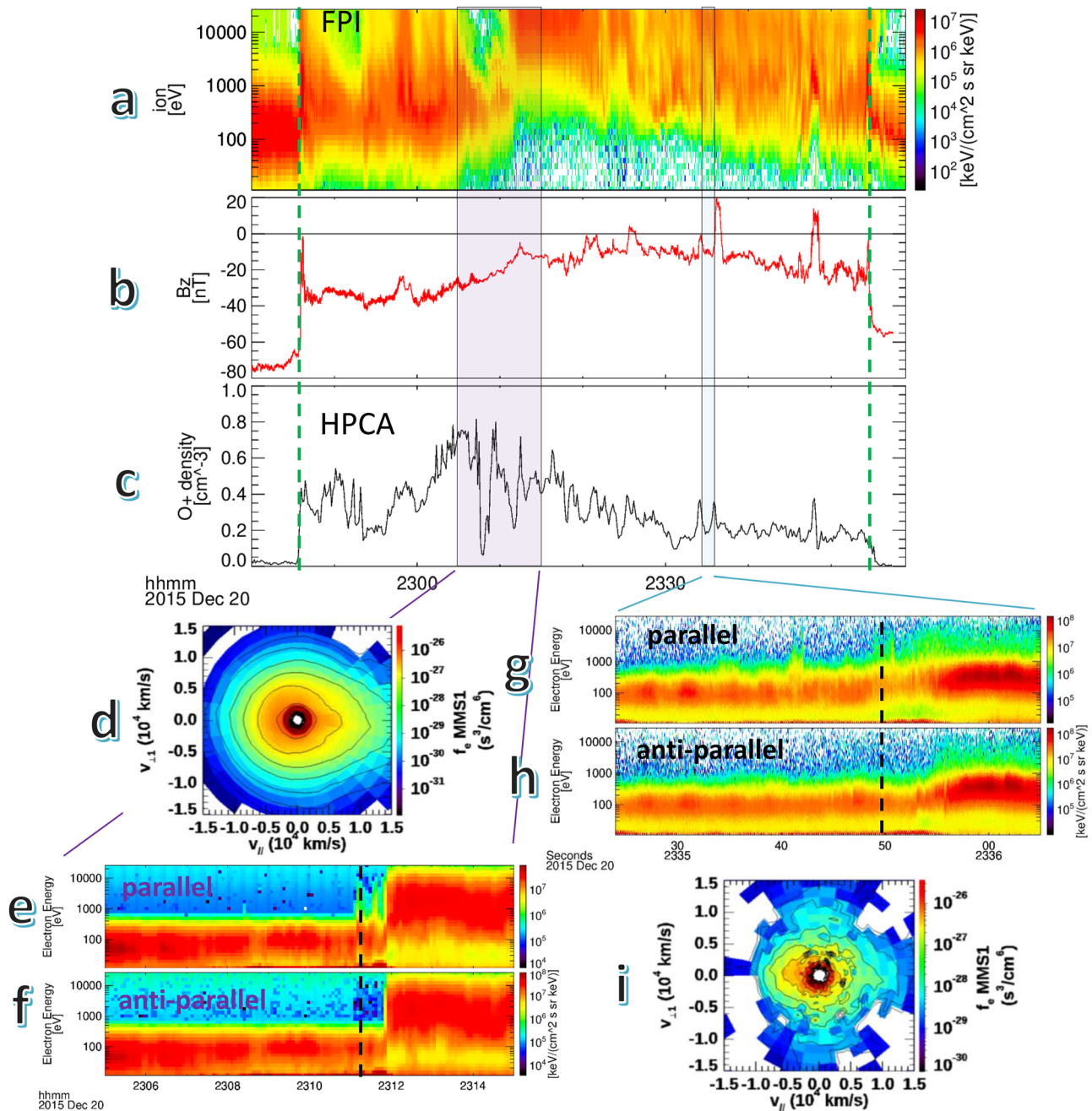
Figure 2. Top panels show Fast Plasma Investigation (FPI) omni-directional ion spectrogram (a), Fluxgate Magnetometer B_z in geocentric solar magnetospheric coordinates (b), and Hot Plasma Composition Analyzer O+ density (c), from 22:40 to 22:59 UT 12/20. The electron velocity distributions (d) at 23:11:10.802 UT (fast mode) and (i) at 23:35:49.843 UT (burst mode) are from intervals of uni-directional greater than 1 keV electrons. Accompanying FPI electron parallel and anti-parallel energy spectrograms are zoomed-in to the time periods 23:05–23:15 UT (e and f) and burst data 23:35:24–23:36:05 UT (g and h).

with magnetized electrons with $V_i < V_{e\perp} \sim V_{ExB}$ (Figure 3i). These features combined support that the density minima are magnetic separatrices.

Multiple features support the interpretation that MMS encountered the magnetosphere side of the reconnection inflow region near the secondary reconnection x-line during the interval 23:35:56-23:36:02 UT in Figure 3. This interpretation is founded on: (a) electron velocity distributions exhibit the characteristic temperature anisotropy ($T_{e\parallel} > T_{e\perp}$) with parallel elongation (Figures 3l, 3m), an outstanding feature of the magnetosphere inflow in the ion diffusion region (IDR) as predicted by particle-in-cell simulations (Figure 3j in Chen, Hesse, Wang,
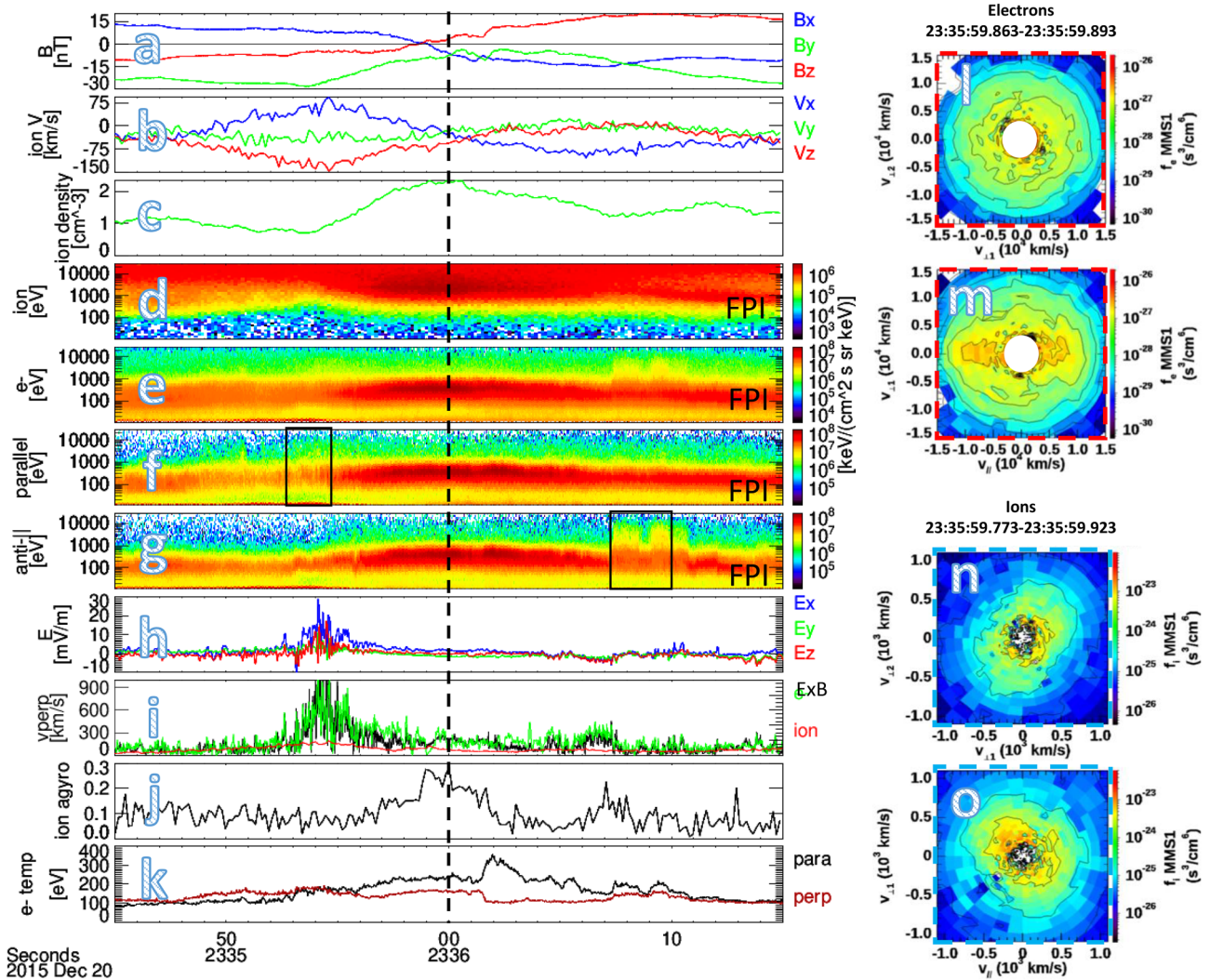
Figure 3. Signatures of nearby reconnection observed in the second encounter of positive B_z embedded in BL2. Panels show magnetic field (a), ion velocity (b), ion density (c), omni-directional ion (d) and electron (e) spectrograms, parallel (f) and anti-parallel (g) electron spectrograms, electric field (h), magnetic field perpendicular velocity of (red) ions (green) electrons, and (black) $\mathbf{E} \times \mathbf{B}$ drift speed (i), ion agyrotropy (see Scudder and Daughton (2008), panel (j)), parallel (black) and perpendicular (brown) electron temperatures (k). Vector quantities are in geocentric solar magnetospheric coordinates. Panels (l–o) show burst velocity distributions observed at the vertical dashed line, with electron(ion) distributions outlined by a red(blue) dashed square (⊥2 is the cross product of the magnetic field parallel direction and ⊥1 direction). The black box in panels (f and g) shows uni-directional electrons at the magnetic separatrix.

Gershman, et al. (2016); Figure 2/panels h6 and j6 in Chen, Hesse, Wang, Bessho, et al. (2016); Le et al. (2017)) and observed in previous magnetopause diffusion region encounters (Figure 3d in Chen, Hesse, Wang, Gershman, et al. (2016); Figure 3i in Chen et al. (2017)). (b) Non-gyrotropic ions (Figures 3j, 3n and 3o) as expected for the magnetospheric side of the reconnection inflow (S. Wang et al., 2016). (c) The ion flow perpendicular to the magnetic field is decoupled from the electron and $\mathbf{E} \times \mathbf{B}$ flows and exhibits the expected ordering in an IDR with $V_i < V_{e\perp} \sim V_{ExB}$. These observations are consistent with MMS sampling the IDR but this interpretation is not a unique possibility to account for the observed features. A thin layer of ions just inside of the magnetopause can exhibit nongyrotropy as the ions are remotely sensed.

The proximity of MMS to the reconnection x-line presents observational support for secondary reconnection equatorward and not too far from the southern cusp, given the magnetosphere exit into BL2 under $B_z < 0$ approximately 15 min before. The increasing $T_{e\parallel}$ and decreasing $T_{e\perp}$ (Figure 3k) are consistent with the trend expected for the reconnection diffusion region just upstream of the electron reconnection layer (Chen et al., 2009). This feature is caused by a combination of parallel acceleration by the potential drop and perpendicular cooling due
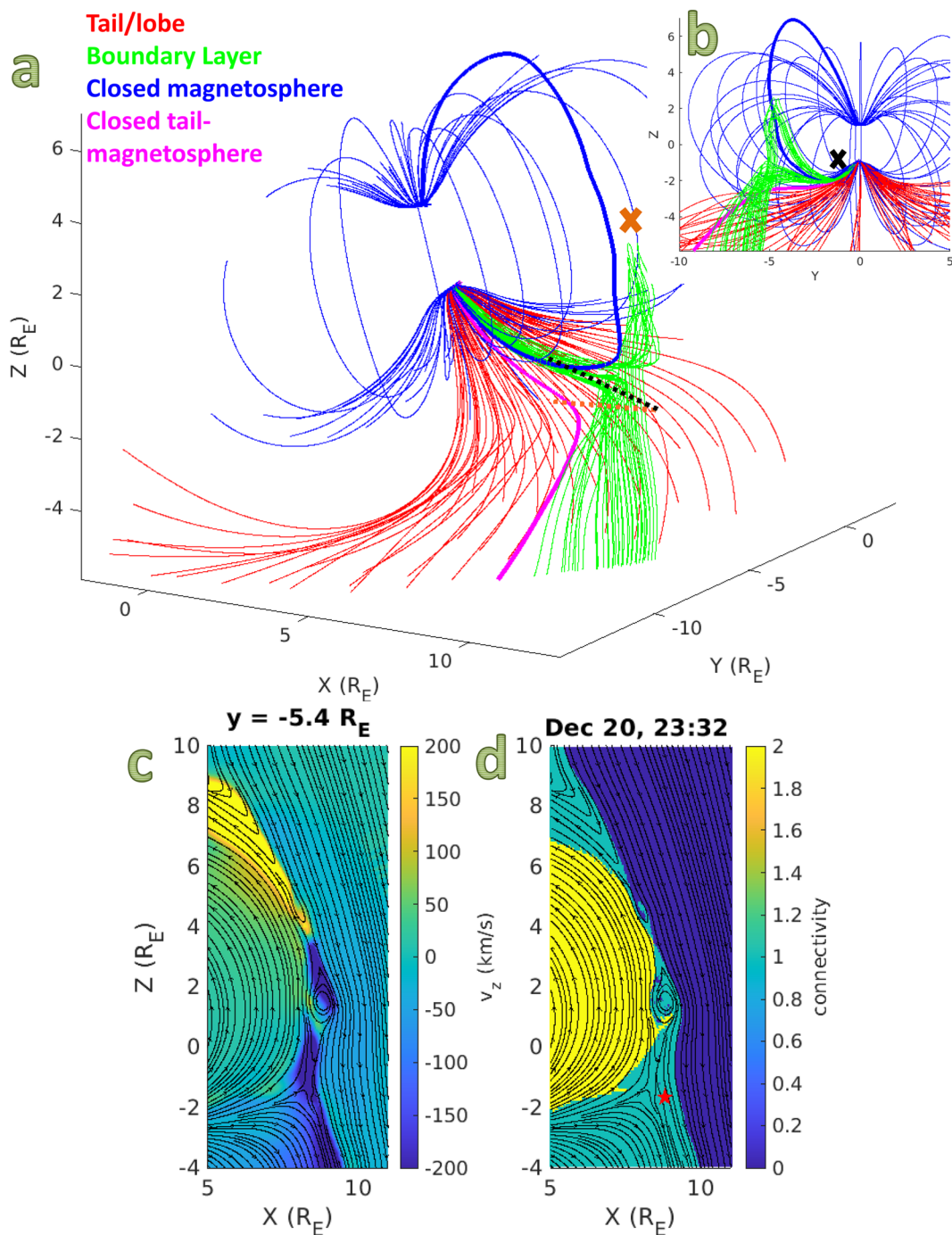
Figure 4. Panel (a) shows an oblique view of the cusp and surrounding 3D field lines in the global simulation at 23:32 UT 12/20. Simulation results are presented in geocentric solar magnetospheric coordinates. Red represents lobe field lines, blue closed magnetosphere, and green the magnetopause boundary layer (BL) field lines (see text for how they are defined in the simulation). The black dashed trajectory demonstrates scenario 1, where Magnetospheric Multi-Scale (MMS) traverses from BL1 to magnetosphere (see highlighted Figure 1) equatorward of the southern cusp. The orange dashed trajectory demonstrates scenario 2, showing MMS crossing from BL1 into the magnetosphere tailward of the southern cusp. The magenta curve is drawn manually to illustrate a closed magnetosphere field line extending to the near-earth magnetotail (Johnson et al., 2021; Petrinec et al., 2022). Panel (b) shows the same field lines viewed in the y–z plane. Orange and black x symbols, in panels (a and b) respectively, represent different reconnection locations to account for observed unidirectional streaming electrons. Panels (c and d) show cuts at y = −5.4 R_E. Panel (c) shows v_z and (d) shows magnetic connectivity (0 = open-open, 1 = open-closed, 2 = closed-closed). In Panels (c and d), black field lines are traced in the 2D plane. The red star indicates position of MMS. Note the thin yellow region branching out under the flux rope, indicating closed magnetic flux extending into the BL.

to conservation of the first adiabatic invariant ($mv_\perp^2/B$). Figure 3d also shows a strong flux of ions with energies >10 keV, and Figure 3e shows electrons in this region are a mixture of energized magnetosheath and magnetosphere electrons, similar to previous MMS diffusion region crossings in the magnetosphere side (e.g., Figures 2a and 2b in Ergun et al. (2017)). In contrast, when MMS exited the magnetosphere around 23:36:50 UT (see Figure S1 in Supporting Information S1), similar reconnection signatures were not observed, which suggests that MMS may have been in close proximity to the reconnection x-line only during the crossing around 23:36:00, due to motions of the secondary reconnection site.

3. Global MHD Simulation

We have simulated the 2015 winter solstice storm using the Grid Agnostic magnetohydrodynamics (MHD) for Extended Research Applications global magnetosphere simulation (Sorathia et al., 2020; Zhang et al., 2019), using OMNI data as solar wind input. The simulation includes from 12:00 UT 12/19 to the end of 12/20, preconditioning the magnetosphere with 30+ hr of observed solar wind parameters during this storm to compare with MMS observations. This preconditioning is expected to provide a more realistic state of the magnetosphere than a steady state model (Borovsky & Steinberg, 2006).

Fully three-dimensional magnetic field lines emanating from the southern cusp and surrounding regions are shown from the global simulation in Figure 4a. Red field lines represent southern lobe flux, which extend to 40 R_E down-tail without closing in the northern hemisphere, blue field lines the closed day-side magnetosphere, and green field lines the magnetopause BL. Green field lines map both the magnetospheric and magnetosheath sides of exhausted flux, and some of them map far north of the southern cusp around the flux rope structure visible in Figures 4c and 4d. The simulation time is 23:32 UT. Since it is not possible to capture the time-dependent expansion and contraction of the magnetospheric boundaries in a single snapshot, the dashed black line is an example trajectory showing where MMS encountered magnetospheric field lines with $B_z < 0$ (note blue field line nearest green BL field lines). The example trajectory (moving from right to left) shows MMS in the magnetosheath, then BL, then magnetosphere, corresponding to the first three colored highlighting regions from Figure 1: the time interval 22:10–23:20 UT.

Secondary reconnection is identified in the simulation near the southern cusp, and it produces closed flux in the BL. An example is illustrated in Figures 4c and 4d using simulation cuts at the y-coordinate of MMS ($y = -5.4\ R_E$) and at 23:32 UT 12/20. Figure 4c is a v_z colormap with black field lines traced in the plane. At $z \sim 3\ R_E$, there is a strong flow reversal associated with the primary x-line. Another flow reversal occurs around $z = 0\ R_E$ due to secondary reconnection in the vicinity of the southern cusp. Figure 4d shows the magnetic connectivity. The value 0 means no connection to the inner boundary of the simulation (ionosphere) at $r = 2\ R_E$, 1 means a single end of the field line connects to the ionosphere, and 2 means both ends connect to the ionosphere. In the region around $z = 0\ R_E$, the secondary reconnection jet is associated with closed flux (yellow) extending into the BL and just below some dark blue patches (open to the solar wind at both ends) where the flux rope is sliced. Observations together with the simulation exemplify the occurrence of multiple reconnection sites along the magnetopause, and the potential formation of flux transfer events (e.g., Southwood et al., 1988), which are flux ropes with a mixture of open-open, closed-closed, and open-closed field lines (Lv et al., 2016).

Whether a spacecraft can remain in the closed portion of the BL for a long time depends on many factors, such as how fast the boundary moves, its thickness, and any warping. Around the simulation time presented in Figure 4, secondary reconnection sites are transient. They are sometimes closer to/farther from the cusps than shown in the time-step and y-plane in Figure 4. A time series of simulation snapshots indicate that flux ropes formed by secondary reconnection move toward the cusp and MMS. This time step is most illustrative because it is at the same y-coordinate as MMS and shows a significant region of closed field extending into the BL. The red star in Figure 4d shows the MMS formation is farther south than the secondary reconnection.

4. Summary

We report an MMS crossing from the magnetosheath into magnetosphere, in-between which it sampled multiple BLs with different properties, approximately at the peak ring current of a large geomagnetic storm near winter solstice. These wide magnetopause BLs associated with low Mach number storm-time and large dipole tilt, and containing closed flux regions, are similar to those reported forming due to remote reconnection (Paschmann

et al., 2021). The key new feature in our event is the entry into the magnetosphere with $B_z < 0$, interpreted as MMS crossing from BL1 through the magnetopause either equatorward or tailward of the southern cusp. In addition, Paschmann et al. (2021) hypothesized that higher latitude reconnection occurred to produce closed field lines in the BL. In this study, observational evidence indicates consistency with a reconnection x-line near the southern cusp as MMS crossed from BL1 into the magnetosphere, supporting active reconnection nearby. Furthermore, the global MHD simulation shows secondary reconnection in the vicinity of the southern cusp and MMS during the time period of interest. Field line tracing reveals regions of closed flux in the BL adjacent to the secondary reconnection jets. Our observation and simulation results both support the hypothesis by Paschmann et al. (2021), even though how the time-dependent secondary reconnection process commences to form closed flux regions of flux ropes remains an open question.

One important implication of our results is that the cusp plasma can be of lower density and higher energy than the magnetosheath plasma during geomagnetic storms. The standard picture is that the cusp is filled with magnetosheath plasma, being formed by reconnection between IMF field lines and magnetospheric field lines. However, the storm-time BLs, which would ultimately be the source for cusp plasma, contain plasma that is more energetic than the magnetosheath during this event (BL1 and BL2 in Figure 1). The O+ signatures further indicate the presence of magnetospheric plasma in the BL. Secondary reconnection is capable of energizing the BL plasma to another level, and may account for the observation that BL2 contains more energetic plasmas than BL1. Our results indicate that using magnetosheath plasma characteristics to identify the cusp, such as that implemented for automatic detection of cusp ion dispersion events (da Silva et al., 2022), requires further validation for storm times.

Data Availability Statement

All of the data for this study are available from the NASA Space Physics Data Facility https://cdaweb.gsfc.nasa.gov/. The global MHD simulation outputs at 1-min resolution covering the time period 22:30 UT 12/20 to 00:00 UT 12/21, 2015 are archived at Zenodo https://doi.org/10.5281/zenodo.6780134.

References

Borovsky, J. E., & Steinberg, J. T. (2006). The "calm before the storm" in CIR/magnetosphere interactions: Occurrence statistics, solar wind statistics, and magnetospheric preconditioning. *Journal of Geophysical Research*, *111*(A7), A07S10. https://doi.org/10.1029/2005JA011397

Brenner, A., Pulkkinen, T. I., Al Shidi, Q., & Toth, G. (2021). Stormtime energetics: Energy transport across the magnetopause in a global MHD simulation. *Frontiers in Astronomy and Space Sciences*, *8*, 756732. https://doi.org/10.3389/fspas.2021.756732

Chen, L.-J., Bessho, N., Lefebvre, B., Vaith, H., Asnes, A., Santolik, O., et al. (2009). Multispacecraft observations of the electron current sheet, neighboring magnetic Islands, and electron acceleration during magnetotail reconnection. *Physics of Plasmas*, *16*(5), 056501. https://doi.org/10.1063/1.3112744

Chen, L.-J., Hesse, M., Wang, S., Bessho, N., & Daughton, W. (2016). Electron energization and structure of the diffusion region during asymmetric reconnection. *Geophysical Research Letters*, *43*(6), 2405–2412. https://doi.org/10.1002/2016GL068243

Chen, L.-J., Hesse, M., Wang, S., Gershman, D., Ergun, R., Pollock, C., et al. (2016). Electron energization and mixing observed by MMS in the vicinity of an electron diffusion region during magnetopause reconnection. *Geophysical Research Letters*, *43*(12), 6036–6043. https://doi.org/10.1002/2016GL069215

Chen, L.-J., Hesse, M., Wang, S., Gershman, D., Ergun, R. E., Burch, J., et al. (2017). Electron diffusion region during magnetopause reconnection with an intermediate guide field: Magnetospheric multiscale observations. *Journal of Geophysical Research: Space Physics*, *122*(5), 5235–5246. https://doi.org/10.1002/2017JA024004

Cowley, S. W. H. (1982). The causes of convection in the Earth's magnetosphere: A review of developments during the IMS. *Reviews of Geophysics*, *20*(3), 531–565. https://doi.org/10.1029/RG020i003p00531

da Silva, D., Chen, L. J., Fuselier, S., Wang, S., Elkington, S., Dorelli, J., et al. (2022). Automatic identification and new observations of ion energy dispersion events in the cusp ionosphere. *Journal of Geophysical Research: Space Physics*, *127*(4), e2021JA029637. https://doi.org/10.1029/2021JA029637

Eastman, T. E., & Hones, E. W., Jr. (1979). Characteristics of the magnetospheric boundary layer and magnetopause layer as observed by IMP 6. *Journal of Geophysical Research*, *84*(A5), 2019–2028. https://doi.org/10.1029/JA084iA05p02019

Ergun, R. E., Chen, L.-J., Wilder, F. D., Ahmadi, N., Eriksson, S., Usanova, M. E., et al. (2017). Drift waves, intense parallel electric fields, and turbulence associated with asymmetric magnetic reconnection at the magnetopause. *Geophysical Research Letters*, *44*(7), 2978–2986. https://doi.org/10.1002/2016GL072493

Farrugia, C. J., Lugaz, N., Alm, L., Vasquez, B., Argall, M. R., Kucharek, H., et al. (2017). MMS observations of reconnection at dayside magnetopause crossings during transitions of the solar wind to sub-Alfvénic flow. *Journal of Geophysical Research: Space Physics*, *122*(10), 9934–9951. https://doi.org/10.1002/2017JA024563

Fuselier, S. A., Anderson, B. J., & Onsager, T. G. (1997). Electron and ion signatures of field line topology at the low-shear magnetopause. *Journal of Geophysical Research*, *102*(A3), 4847–4863. https://doi.org/10.1029/96JA03635

Fuselier, S. A., Mukherjee, J., Denton, M. H., Petrinec, S. M., Trattner, K. J., Toledo-Redondo, S., et al. (2019). High-density O+ in Earth's outer magnetosphere and its effect on dayside magnetopause magnetic reconnection. *Journal of Geophysical Research: Space Physics*, *124*(12), 10257–10269. https://doi.org/10.1029/2019JA027396

Johnson, J. R., Wing, S., Delamere, P., Petrinec, S., & Kavosi, S. (2021). Field-aligned currents in auroral vortices. *Journal of Geophysical Research: Space Physics*, *126*(2), e2020JA028583. https://doi.org/10.1029/2020JA028583

Lavraud, B., Zhang, Y. C., Vernisse, Y., Gershman, D. J., Dorelli, J., Cassak, P. A., et al. (2016). Currents and associated electron scattering and bouncing near the diffusion region at Earth's magnetopause. *Geophysical Research Letters*, *43*(7), 3042–3050. https://doi.org/10.1002/2016GL068359

Le, A., Daughton, W., Chen, L.-J., & Egedal, J. (2017). Enhanced electron mixing and heating in 3-D asymmetric reconnection at the Earth's magnetopause. *Geophysical Research Letters*, *44*(5), 2096–2104. https://doi.org/10.1002/2017GL072522

Li, L. Y., Cao, J. B., Zhou, G. C., Zhang, T. L., Zhang, D., Dandouras, I., et al. (2011). Multiple responses of magnetotail to the enhancement and fluctuation of solar wind dynamic pressure and the southward turning of interplanetary magnetic field. *Journal of Geophysical Research*, *116*(A12), A12223. https://doi.org/10.1029/2011JA016816

Lv, L. Q., Pu, Z., & Xie, L. (2016). Multiple magnetic topologies in flux transfer events: THEMIS measurements. *Science China Technological Sciences*, *59*(8), 1283–1293. https://doi.org/10.1007/s11431-016-6071-9

Maynard, N. C., Aggson, T. L., Basinska, E. M., Burke, W. J., Craven, P., Peterson, W. K., et al. (1991). Magnetospheric boundary dynamics: DE 1 and DE 2 observations near the magnetopause and cusp. *Journal of Geophysical Research*, *96*(A3), 3505–3522. https://doi.org/10.1029/90JA02167

Michael, A. T., Sorathia, K. A., Merkin, V. G., Nykyri, K., Burkholder, B., Ma, X., et al. (2021). Modeling Kelvin-Helmholtz instability at the high-latitude boundary layer in a global magnetosphere simulation. *Geophysical Research Letters*, *48*(19), e2021GL094002. https://doi.org/10.1029/2021GL094002

Mitchell, D. G., Kutchko, F., Williams, D. J., Eastman, T. E., Frank, L. A., & Russell, C. T. (1987). An extended study of the low-latitude boundary layer on the dawn and dusk flanks of the magnetosphere. *Journal of Geophysical Research*, *92*(A7), 7394–7404. https://doi.org/10.1029/JA092iA07p07394

Nakamura, T. K. M. (2021). The Earth's low-latitude boundary layer. In *Magnetospheres in the solar system* (pp. 177–191). American Geophysical Union (AGU). https://doi.org/10.1002/9781119815624.ch12

Nowada, M., Shue, J.-H., & Russell, C. (2009). Effects of dipole tilt angle on geomagnetic activity. *Planetary and Space Science*, *57*(11), 1254–1259. https://doi.org/10.1016/j.pss.2009.04.007

Paschmann, G., Sonnerup, B. U. O., Phan, T., Fuselier, S. A., Haaland, S., Denton, R. E., et al. (2021). Anomalous reconnection layer at Earth's dayside magnetopause. *Journal of Geophysical Research: Space Physics*, *126*(9), e2021JA029678. https://doi.org/10.1029/2021JA029678

Petrinec, S. M., Wing, S., Johnson, J. R., & Zhang, Y. (2022). Multi-spacecraft observations of fluctuations occurring along the dusk flank magnetopause, and testing the connection to an observed ionospheric bead. *Frontiers in Astronomy and Space Sciences*, *9*, 827612. https://doi.org/10.3389/fspas.2022.827612

Reyes, P. I., Pinto, V. A., & Moya, P. S. (2021). Geomagnetic storm occurrence and their relation with solar cycle phases. *Space Weather*, *19*(9), e2021SW002766. https://doi.org/10.1029/2021SW002766

Scudder, J., & Daughton, W. (2008). "Illuminating" electron diffusion regions of collisionless magnetic reconnection using electron agyrotropy. *Journal of Geophysical Research*, *113*(A6), A06222. https://doi.org/10.1029/2008JA013035

Shuster, J. R., Chen, L.-J., Daughton, W. S., Lee, L. C., Lee, K. H., Bessho, N., et al. (2014). Highly structured electron anisotropy in collisionless reconnection exhausts. *Geophysical Research Letters*, *41*(15), 5389–5395. https://doi.org/10.1002/2014GL060608

Shuster, J. R., Gershman, D. J., Chen, L.-J., Wang, S., Bessho, N., Dorelli, J. C., et al. (2019). MMS measurements of the Vlasov equation: Probing the electron pressure divergence within thin current sheets. *Geophysical Research Letters*, *46*(14), 7862–7872. https://doi.org/10.1029/2019GL083549

Sonnerup, B. U. O. (1971). Magnetopause structure during the magnetic storm of September 24, 1961. *Journal of Geophysical Research*, *76*(28), 6717–6735. https://doi.org/10.1029/JA076i028p06717

Sorathia, K. A., Merkin, V. G., Panov, E. V., Zhang, B., Lyon, J. G., Garretson, J., et al. (2020). Ballooning-interchange instability in the near-Earth plasma sheet and auroral beads: Global magnetospheric modeling at the limit of the MHD approximation. *Geophysical Research Letters*, *47*(14), e2020GL088227. https://doi.org/10.1029/2020GL088227

Southwood, D., Farrugia, C., & Saunders, M. (1988). What are flux transfer events? *Planetary and Space Science*, *36*(5), 503–508. https://doi.org/10.1016/0032-0633(88)90109-2

Wang, C., Huang, Z., Hu, Y., & Guo, X. (2005). 3D global simulation of the interaction of interplanetary shocks with the magnetosphere. *AIP Conference Proceedings*, *781*(1), 320–324. https://doi.org/10.1063/1.2032716

Wang, S., Chen, L.-J., Hesse, M., Bessho, N., Gershman, D. J., Dorelli, J., et al. (2016). Two-scale ion meandering caused by the polarization electric field during asymmetric reconnection. *Geophysical Research Letters*, *43*(15), 7831–7839. https://doi.org/10.1002/2016GL069842

Zhang, B., Sorathia, K. A., Lyon, J. G., Merkin, V. G., Garretson, J. S., & Wiltberger, M. (2019). GAMERA: A three-dimensional finite-volume MHD solver for non-orthogonal curvilinear geometries. *The Astrophysical Journal – Supplement Series*, *244*(1), 20. https://doi.org/10.3847/1538-4365/ab3a4c

References From the Supporting Information

Blake, J. B., Mauk, B. H., Baker, D. N., Carranza, P., Clemmons, J. H., Craft, J., et al. (2016). The fly's eye energetic particle spectrometer (FEEPS) sensors for the magnetospheric multiscale (MMS) mission. *Space Science Reviews*, *199*(1), 309–329. https://doi.org/10.1007/s11214-015-0163-x

Burch, J. L., Moore, T. E., Torbert, R. B., & Giles, B. L. (2016). Magnetospheric multiscale overview and science objectives. *Space Science Reviews*, *199*(1), 5–21. https://doi.org/10.1007/s11214-015-0164-9

Ergun, R. E., Tucker, S., Westfall, J., Goodrich, K. A., Malaspina, D. M., Summers, D., et al. (2016). The axial double probe and fields signal processing for the MMS mission. *Space Science Reviews*, *199*(1), 167–188. https://doi.org/10.1007/s11214-014-0115-x

Lindqvist, P. A., Olsson, G., Torbert, R. B., King, B., Granoff, M., Rau, D., et al. (2016). The spin-plane double probe electric field instrument for MMS. *Space Science Reviews*, *199*(1–4), 17–165. https://doi.org/10.1007/s11214-014-0116-9

Pollock, C., Moore, T., Jacques, A., Burch, J., Gliese, U., Saito, Y., et al. (2016). Fast plasma investigation for magnetospheric multiscale. *Space Science Reviews*, *199*(1), 331–406. https://doi.org/10.1007/s11214-016-0245-4

Torbert, R. B., Russell, C. T., Magnes, W., Ergun, R. E., Lindqvist, P.-A., LeContel, O., et al. (2016). The fields instrument suite on MMS: Scientific objectives, measurements, and data products. *Space Science Reviews*, *199*(1), 105–135. https://doi.org/10.1007/s11214-014-0109-8

Young, D. T., Burch, J. L., Gomez, R. G., De Los Santos, A., Miller, G. P., Wilson, P., et al. (2016). Hot plasma composition analyzer for the magnetospheric multiscale mission. *Space Science Reviews*, *199*(1), 407–470. https://doi.org/10.1007/s11214-014-0119-6